International Journal of Extreme Manufacturing

PAPER • **OPEN ACCESS**

Multifunctional and reprogrammable 4D pixel mechanical metamaterials

To cite this article: Xiaozhou Xin *et al* 2025 *Int. J. Extrem. Manuf.* **7** 015506

View the article online for updates and enhancements.

You may also like

- Advancements in 3D skin bioprinting: processes, bioinks, applications and sensor integration
I Deniz Derman, Taino Rivera, Laura Garriga Cerda et al.

- A review for design, mechanism, fabrication, and application of magnetically responsive microstructured functional surface
Jian Wang, Xingyi Song, Chaochao Wang et al.

- Programmable mechanical properties of additively manufactured novel steel
Jinlong Su, Qian Li, Jie Teng et al.

This content was downloaded from IP address 111.40.58.207 on 14/05/2025 at 04:34

OPEN ACCESS
IOP Publishing | IMMT International Journal of Extreme Manufacturing
Int. J. Extrem. Manuf. 7 (2025) 015506 (14pp) https://doi.org/10.1088/2631-7990/ad884a

Multifunctional and reprogrammable 4D pixel mechanical metamaterials

Xiaozhou Xin[1], Cheng Lin[2], Bingxun Li[1], Ruikang Zhang[2], Chengjun Zeng[1], Liwu Liu[1,*], Yanju Liu[1,*] and Jinsong Leng[2]

[1] Department of Astronautical Science and Mechanics, Harbin Institute of Technology (HIT), PO Box 301, No. 92 West Dazhi Street, Harbin 150001, People's Republic of China
[2] Center for Composite Materials and Structures, Harbin Institute of Technology (HIT), PO Box 3011, No. 2 Yikuang Street, Harbin 150080, People's Republic of China

E-mail: liulw@hit.edu.cn and yj_liu@hit.edu.cn

Received 18 February 2024, revised 20 May 2024
Accepted for publication 16 October 2024
Published 14 November 2024

Abstract
Metamaterials have exotic physical properties that rely on the construction of their underlying architecture. However, the physical properties of conventional mechanical metamaterials are permanently programmed into their periodic interconnect configurations, resulting in their lack of modularity, scalable fabrication, and programmability. Mechanical metamaterials typically exhibit a single extraordinary mechanical property or multiple extraordinary properties coupled together, making it difficult to realize multiple independent extraordinary mechanical properties. Here, the pixel mechanics metamaterials (PMMs) with multifunctional and reprogrammable properties are developed by arraying uncoupled constrained individual modular mechanics pixels (MPs). The MPs enable controlled conversion between two extraordinary mechanical properties (multistability and compression-torsion coupling deformation). Each MP exhibits 32 independent and reversible room temperature programming configurations. In addition, the programmability of metamaterials is further enhanced by shape memory polymer (SMP) and 4D printing, greatly enriching the design freedom. For the PMM consisting of $m \times n$ MPs, it has $32^{(m \times n)}$ independent room temperature programming configurations. The application prospects of metamaterials in the vibration isolation device and energy absorption device with programmable performance have been demonstrated. The vibration isolation frequencies of the MP before and after programming were [0 Hz–5.86 Hz], [0 Hz–13.67 Hz and 306.64 Hz–365.23 Hz]. The total energy absorption of the developed PMM can be adjusted controllably in the range of 1.01 J–3.91 J. Six standard digital logic gates that do not require sustained external force are designed by controlling the closure between the modules. This design paradigm will facilitate the further development of multifunctional and reprogrammable metamaterials.

* Authors to whom any correspondence should be addressed.

Original content from this work may be used under the terms of the Creative Commons Attribution 4.0 licence. Any further distribution of this work must maintain attribution to the author(s) and the title of the work, journal citation and DOI.

© 2024 The Author(s). Published by IOP Publishing Ltd on behalf of the IMMT
2631-7990/25/015506+14$33.00

Supplementary material for this article is available online

Keywords: 4D printing, shape memory polymer, pixel mechanical metamaterials, multistable, compression-twist coupling metamaterials, digital logic gates

1. Introduction

Mechanical metamaterials are complex artificial materials with rational designs that exhibit exotic mechanical properties (e.g. compression-torsion coupling metamaterials, multistable metamaterials), which exhibit diverse configurations and highly designable mechanical properties contributing to the development of intelligent devices [1–13]. The compressive-torsion metamaterials exhibit torsional deformation when subjected to compressive loading, with degree of freedom (DOF) exceeding the Cauchy elasticity [14–16]. Multistable mechanical metamaterials possess two or multiple stable configurations utilizing the buckling phenomenon, and exhibit negative stiffness properties [17–19]. The mechanical properties and deformation characteristics of the mechanical metamaterials depend on the configuration of the cells, which are programmed to the metamaterials in a permanent manner, resulting in its configuration/mechanical properties lacking in adaptivity and reconfigurability [20–24]. Mechanical metamaterials are gradually developing toward multifunctionality, diversity, reprogrammability, and high designability [20].

The rapid rise of 4D printing and smart materials has created opportunities to design mechanical metamaterials with reconfigurable properties [25–30]. Shape memory polymer (SMP) had the ability to maintain a temporary configuration and recover to its original configuration in response to external stimuli, such as heat, light, electricity, magnetism, etc [31–34]. 4D printing was enabled by 3D printing the SMP, and the configuration/performance of the printed object could be changed over time [35–41]. 4D printed mechanical metamaterials combined structure-optimized design with the stimulus-responsive properties of the materials, endowing it with programmable, reconfigurable, and multifunctional properties, further enriching the design freedom of metamaterials. 4D printing origami structures, lattice structures, auxetic structures, multistable structures, and compression-torsion coupling metamaterials with reconfigurable properties have been developed, demonstrating promising application prospects in reconfigurable energy-absorbing structures, flexible electronics, and medical devices [15, 16, 24, 42, 43].

However, the stimuli-responsive mechanical metamaterials were usually composed of periodically interconnected microstructure, which restricted the modularity and scalable manufacturing of metamaterials. It also led to these materials possessing only a single extraordinary mechanical property or coupled with multiple extraordinary mechanical properties. To break through this limitation, multifunctional and reprogrammable pixel mechanical metamaterials (PMMs) were developed in this work. The core requirements of the developed mechanical metamaterials were as follows: (*i*) metamaterials have two independent and decoupled extraordinary mechanical properties, and can be transformed according to requirements; (*ii*) metamaterials have modular and scalable fabrication properties, and their configurations and mechanical behaviors can be quickly adjusted; (*iii*) metamaterials can be reprogrammed, and the resolution of the programming should be at the level of the individual unit cell, independent of any interactions with adjacent cells.

The concept of PMM originates from the uncoupled deformed array structures of organisms in nature, such as hedgehog spines. Hedgehog spines can effectively absorb the impact of dropping from the height of 10 m [16, 19]. Since the spines were not connected to each other, the damage of one spine did not spread to the other spines, which effectively prevents further damage, figure 1(a). Similar to adjusting a screen image by changing pixel colors, the mechanical properties and configuration of the PMM were adjusted by changing the geometric configuration and spatial arrangement of the individual components (i.e. mechanics pixels, MPs), figure 1(b). PMM endowed mechanical metamaterials with modular design and maintainability. However, the MPs were fabricated monolithically in the reported work on PMMs, resulting in the lack of modularity and scalable fabrication of the MPs.

To address the problem of mechanical metamaterials suffering from the single extraordinary property (or multiple extraordinary properties coupled), the lack of modularity, and scalable fabrication capability, the multifunctional and reprogrammable PMM were developed in this work by arraying modularized MPs. Each MP contained the bistable modules, the 4D-printed compression-torsion modules, and the force threshold control modules, which were mortise-and-tenon jointed to realize its modularity and scalable fabrication. The developed PMM was capable of controllable and reversible transformation in multistable deformation and compression-torsion coupling deformation by controlling the force threshold without employing any electronic devices. Each MP exhibited 32 independent and reversible room temperature programmable configurations, and the integrated PMM had $32^{(m \times n)}$ independent programmable configurations. The contribution of SMP and 4D printing further enhanced the programmability of the metamaterials (in terms of configuration and mechanical properties). Compared with our previous work [16], the MP developed in this work consisted of multiple modules connected by mortise-and-tenon, which enabled modular and scalable fabrication of the MP. Compared to programming the configuration and properties of PMMs through multistable deformation [19], the mechanical metamaterials fabricated by 4D printing exhibited a wider tunable domain of mechanical properties and a higher DOF in design and fabrication. The feasibility of this design strategy was demonstrated through experiments and finite element analysis (FEA), and the potential applications in vibration isolation, logic gates, and energy absorption devices were also demonstrated.

2. Results and discussion

2.1. Design and fabrication of the 4D PMMs

Inspired by the array pattern of hedgehog spines, multi-functional and reprogrammable 4D PMMs with uncoupled deformation between individual components, i.e., MPs, were developed by tiling (m, n) MPs along the (x, y) directions, figure 1(c). The MPs were assembled from 8 modular parts containing three bistable modules (parts 4, 5, and 6), two compression-torsion modules (parts 7 and 8), two force threshold control modules (parts 10 and 11) and a support module, figure 1(d). The support module contained the foundation (part 9), loading end (part 1), bearing (release of the torsional deformation constraint, part 2), and top cap (part 3). This work innovatively introduced the design concepts of ancient Chinese architecture to provide a completely new strategy for scalable fabrication and modular design of metamaterials by utilizing mortise and tenon. The MP modules were connected by mortise and tenon joints, which could be rapidly disassembled and replaced after assembly and enabled adjustment of the MP configuration and performance (section-S1, supporting information).

The bistable module consisted of 12 sinusoidal curved beams ($y = h_0/2\left[1 - \sin\left(\pi/L_0\left(x - L_0/2\right)\right)\right]$) and nine tenons, which were fabricated by 3D printing thermoplastic polyurethanes (TPU), figures 1(e) and S1(c). Five geometric parameters, L_{0x}, L_{0y}, L_0, t_0, and h_0, determined the configuration and mechanical properties of the bistable module. L_{0x} and L_{0y} were the longitudinal and transverse lengths of the bistable module ($L_{0x} = L_{0y}$), respectively. L_0, t_0, and h_0 represented the length, thickness, and height of the sinusoidal curved beam, respectively (Section-S1, Supporting Information). In compression deformation, the displacement-force curve of the bistable module can be divided into three regions: the elastic range, the range of negative incremental stiffness, and the densification range, figure 1(g). In the initial deformation stage, the bistable module underwent elastic deformation to the maximum force ($F_{\max}$). The sinusoidal curve beams were buckled with a further increase in deformation, and the load decreased with the increase in deformation (i.e. negative incremental stiffness phenomenon) until the minimum force occurred ($F_{\min}$). The load exhibited an increasing trend with a further increase in deformation (i.e. densification). When $F_{\min} > 0$ N, the sinusoidal curve beams recovered to their original configuration after unloading, exhibiting a snap-back behavior. On the contrary, when $F_{\min} < 0$ N, the sinusoidal curve beam configuration can be stabilized in the unloaded state (i.e. snap-through based bistability behavior). The bistable module displayed two local potential energy minima under compression by adjusting the geometric parameters (i.e. $F_{\min} < 0$), which resulted in two stable configurations: the initial configuration and the second stable configuration. Figure 1(g) exhibits the displacement-force curves of the two bistable modules involved in this work, i.e. bistable module *i:* $t_0 = 0.75$ mm, $h_0 = 5$ mm, and bistable module *ii:* $t_0 = 1.25$ mm, $h_0 = 7$ mm, with $F_{\max}$ ~4.28 N and ~22.61 N respectively (section-S2, supporting information).

The compression-torsion module was a 3D chiral structure with compression-torsion coupled deformation properties. It contained nodes, helical ligaments (figure 1(f)), a plug, and a geared rotary stopping device. This module was fabricated by 4D printing poly(lactic acid)- SMP (PLA-SMP). The upper and lower nodes of the compression-torsion module were designed with mortises to enable accurate assembly with the bistable module and the force threshold control module. Helical ligaments inspired by the collagen fiber configuration of biological tissues were introduced into the chiral structure to improve the flexibility of the metamaterials (figure 1(f)). The centerline control equation of the helical ligament was $\mathbf{r} = R_\alpha \cos\left(\omega\vartheta\right)\sin\left(\frac{\vartheta}{2}\right)\mathbf{I}_0 + R_\alpha \sin\left(\omega\vartheta\right)\sin\left(\frac{\vartheta}{2}\right)\mathbf{J}_0 + \xi\,\frac{\vartheta}{2\pi}\mathbf{K}_0$, where ω, R_α, and ξ represented the number of coils, the radius of the centerline, and the distance between the two ends of the ligament, respectively. The other geometric parameters of the compression-torsion module were L and d_0, representing the node spacing and ligament diameter, respectively. The connection mode of the nodes and ligaments was divided into left-handed mode (LH) and right-handed mode (RH), figure S1(b) (section-S1, supporting information). The effective mechanical properties (stress–strain, torsion angle φ-displacement curves) of the compression-torsion module could be designed by adjusting the geometric parameters of the ligament. Figures 1(h) and (i) demonstrate the influence of the geometric parameters on the mechanical properties of the compression-torsion module (*i:* $R_\alpha = 1, \omega = 1$, *RH; ii:* $R_\alpha = 1, \omega = 2$, *RH; iii:* $R_\alpha = 3, \omega = 1$, *RH; iv:* $R_\alpha = 3, \omega = 2$, *RH; v:* $R_\alpha = 1, \omega = 1$, *LH; vi:* $R_\alpha = 1$, $\omega = 2$, *LH*), and the FEA reproduced the experimental results with satisfactory accuracy (section-S2, supporting information). Compared to the nodes, the helical ligaments exhibited lower stiffness and deformation mainly occurred in the ligaments during compression. For the same R_α, the axial stiffness of the helix decreased with the increase of the ω, resulting in a larger effective stiffness for the compression-torsion module with a larger ω. The torsion angle of the compression-torsion module increased with the increase of deformation. The chiral connection mode only affected the torsional direction of the module, and hardly changed its torsional angle (figure 1(i)).

Figure S1(d) exhibits the CAD model of the force threshold control modules (fabricated by 3D printing TPU), consisting of 2 opposing C-shaped beams. The plug insertion/extraction force threshold control module required ~14.52 N/11.81 N, figure S6(e). The combination of the compression-torsion module and the force threshold control module had two states, ON and OFF (figure 1(j)), which enabled switching of the deformation characteristics of the compression-torsion

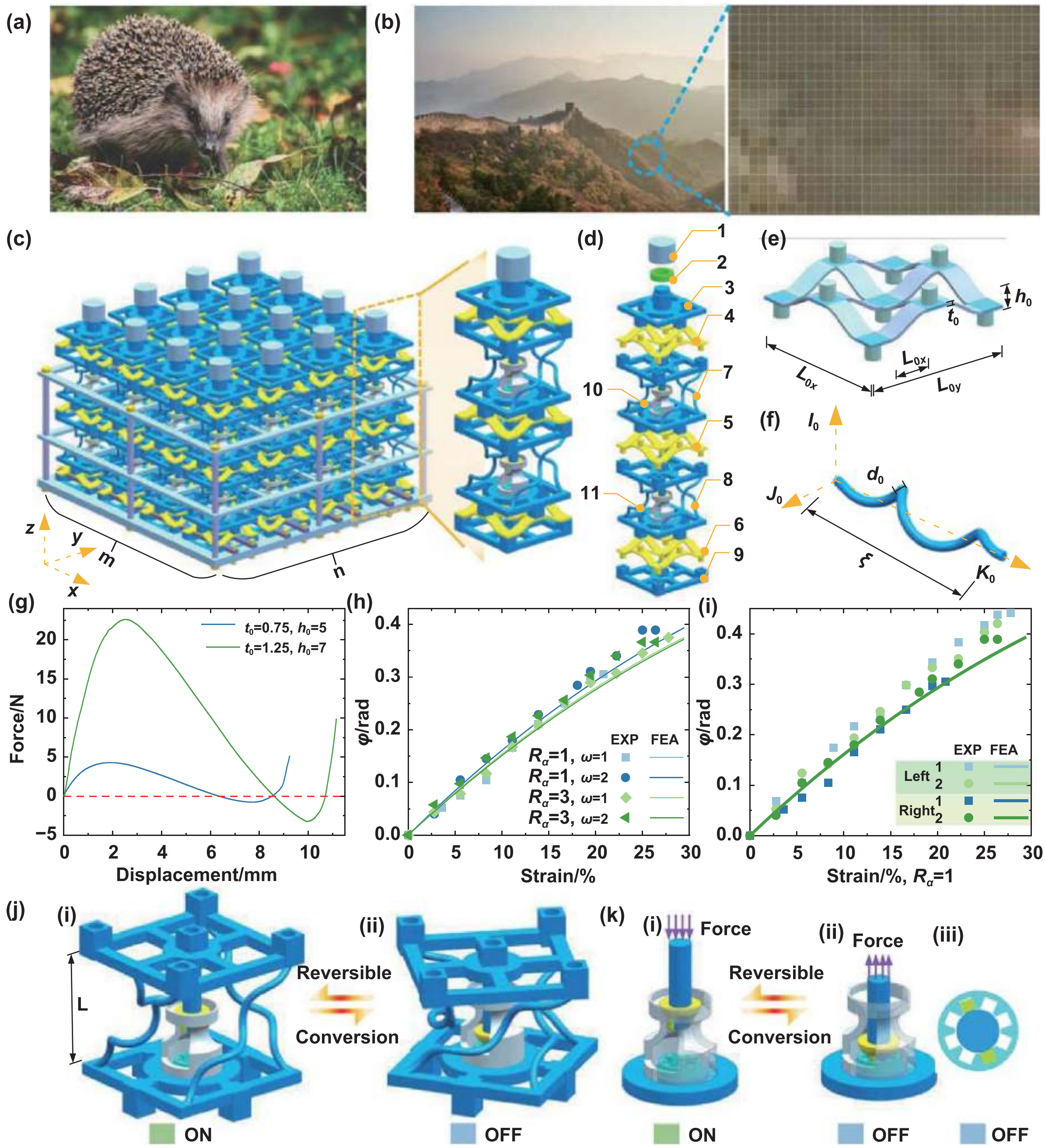

Figure 1. The structural design of the pixel mechanics metamaterial and modules. (a) The spines of a hedgehog are independent. (b) The image of the screen can be tuned by adjusting the color of the pixels. (c) The developed multifunctional and reprogrammable 4D PMM; the PMM consisted of multifunctional and reprogrammable MPs arrays of *m* and *n* MPs in the *x*- and *y*-directions, respectively. (d) Component modules of the MP consisted of: 1 loading end, 2 bearing, 3 top cap, 4–6 bistable module, 7–8 compression-torsion module, 9 foundation, 10–11 force threshold control module. (e) The bistable module. (f) The wavy ligaments inspired by collagen fiber configuration. (g) Displacement-force curves of the bistable modules. (h) and (i) The influence of ligament geometric parameters and chiral modes on the torsional angle-displacement behavior of compression-torsion modules. (j) The ON and OFF states of the combination of the compression-torsion module and the force threshold control module. (i) In the ON state, the compression-torsion module had compression-torsion coupling deformation characteristic; (ii) in the OFF state, the compression-torsion coupling deformation characteristic of the module disappeared. (k) The ON and OFF states of the force threshold control module. (i) In the ON state, the plug was at the upper of the C-shaped beam of the force threshold control module. (ii) In the OFF state, the plug was inserted into the rotary stopping device. (iii) The rotary stopping device and the plug were mutually constrained to limit the torsional deformation.

module, i.e. deformation characteristics with or without compression-torsion coupling. The MP was assembled in the ON state with the plug of the compression-torsion module in contact with the upper of the force threshold control module (figures 1(j–i) and (k–i)). Under compressive deformation, the plug was squeezed through the C-beam to reach the force threshold, and the plug was extruded through the gap between the 2 C-beams until it was inserted into the rotary stopping device, i.e. OFF state (figures 1(j–ii), (k–ii) and (k–iii)). In the ON state, the compression-torsion module had the compression-torsion coupling deformation characteristic. In the OFF state, the bulges of the plug and the recesses in the rotary stopping device constrained each other (figure 1(k–iii)), resulting in the disappearance of the compression-torsion coupling deformation characteristics. During the transition from ON to OFF, the compression-torsion module and the force threshold control module were in the elastic deformation range, causing a reversible transition between these two states.

The stabilization of the bistable modules in the second configuration depended on the strong boundary constraints of the curved beams, which required the interaction and solid connection of the modules during the MP manufacturing process. If there was a large tolerance between the tenon of the prepared bistable module and the mortise of the compression-torsion module, the bistable module was able to transform to the second stable configuration under compressive loading. However, the bistable module would snap-through from the second stable configuration to the initial configuration due to the lack of boundary constraints after unloading. On the contrary, if the modules were connected by interference fit, the individual mortise and tenon joints of the bistable module would not be in the same horizontal position, which led to the tilt of the integrated MP. The connection between the force threshold control module and the compression-torsion module exhibited the same manufacturing difficulties. The force threshold control module was able to control the deformation mode of the MP, which realized the transition between multistable deformation and compression-torsion coupled deformation. In addition, the force threshold control module could also provide guidance for the plug. If the center of the force threshold control module did not coincide with the center of the plug, it could cause the plug to come through the gap in the module during compression deformation, resulting in tilting of the MP. Therefore, higher precision was required for the connection design, fabrication, and assembly of each module.

2.2. Multifunctionality and reprogrammability of the mechanical metamaterials

Ideally, the modules of the MP were deformed sequentially under compression by utilizing the difference in the activation force of the bistable module and the force threshold control module. This resulted in the controlled transformation of MP's deformation mode between the multistable dominant deformation mode and the compression-torsion dominant deformation mode. In this work, eight design examples (MP No. I–VIII) were presented by combining modules with different parameters (bistable module: *i–ii*; compression-torsion module: *i–vi*), as seen in figures 2(a) and (b). Figure 2(c) demonstrates the optical image of the assembled MP.

For the MP with bistable module *i*, the plugs of the compression-torsion module were in contact with the force threshold control module and underwent torsional deformation under compression deformation (Section-S3, Supporting Information). After reaching the activation force $F_{\max}$ of the bistable module, the multistable deformation property of the MP was activated, which caused the dominant deformation mode of the MP to transform from the compression-torsion coupling mode to the multistable deformation mode. When the three bistable modules reached the second stable configuration, the compression-torsion coupling deformation characteristic of the MP was activated as the load reached the force threshold of the force threshold control module. When the plug was inserted into the geared rotary stopping device, the compression-torsion coupling deformation characteristic disappeared (figure 2(d)). In contrast, the MP with bistable module *ii* first reached the threshold force of the force threshold control module, and the MP deformation mode was dominated by compression-torsion coupling. When the plug was inserted into the rotary stopping device, the torsional deformation was constrained, and the compression-torsional deformation characteristic disappeared. The multistable deformation property of the MP was activated with the further increase in deformation (figure 2(e)). In addition, when parts 7 and 8 had different chiral modes, these parts produced same torsional deformation in opposite directions after activation of the force threshold control module, resulting in no torsional deformation at the macroscopic level of the MP (figures 2(f)). Figure 2(g) and S10 exhibit the comparison results of the FEA and experiments of the MP deformation process under different deformations (the parameters as shown in tables 1 and 2). The FEA reproduced the MP deformation process with high accuracy.

Here, the configuration and mechanical properties of the developed MPs could be stably and reversibly programmed at room temperature (i.e. room temperature programming), utilizing the multistable properties and ON/OFF state of the force threshold control module. Each MP possessed 32 independent and stable room temperature programming configurations that were obtained by combining different configuration forms of each module (figure 3(a), section-S3 and movie-S2). The compression properties and vibration isolation characteristics of the MP differed after room temperature programming, owing to the change in its configuration (figures 3(b) and (c)). The developed MP can independently bear external loads in 32 room-temperature programmed configurations, exhibiting different mechanical properties compared to the original configuration, figures 3(b) and S13. For example, when one bistable module was in the second stable configuration, the programmed MP (i.e. No. IV-1-3) first underwent multistable deformation and then reached the threshold of the force threshold control module, activating the compression-torsion coupling deformation characteristics of the MP, figure S13(b). When the 2 compression-torsion modules were turned off, the compression-torsional deformation characteristics of the programmed MP (i.e. No. V-2-1) disappeared and it only maintained the multistable deformation characteristics, figure S13(c). The vibration isolation frequency range of the MP No. IV with the unprogrammed configuration, i.e., No. IV-0, was 0 Hz–5.86 Hz, figure 3(c). When the two bistable

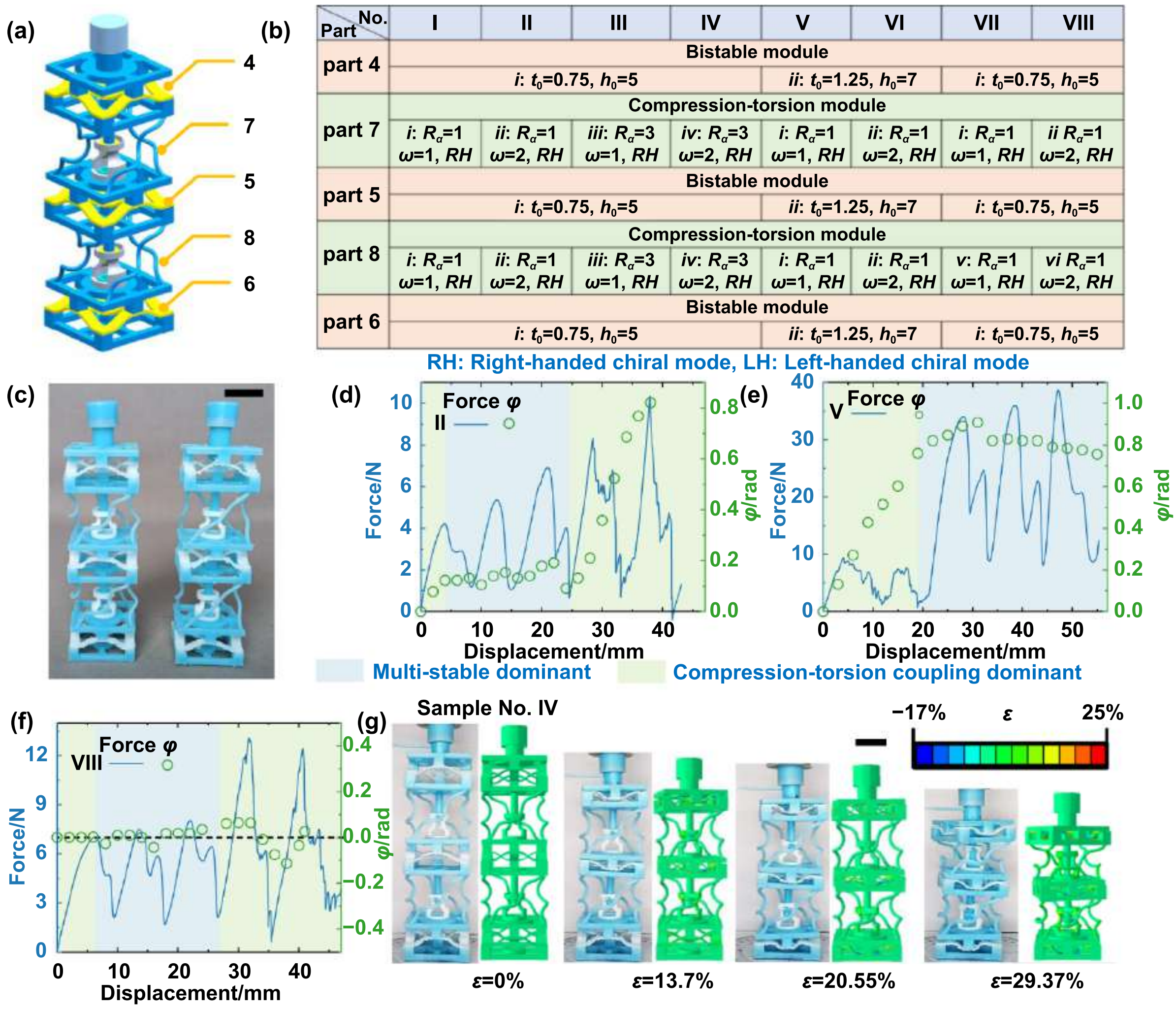

Figure 2. Mechanical properties of the MP. (a) The MP was adjustable mechanically by replacing the bistable and compression-torsion modules. (b) Eight MPs were designed by combining bistable modules (i) and (ii) and compression-torsion modules (i)–(iv). (c) The fabricated MPs (No. IV and II, from left to right). The load-torsion angle-displacement curves of the MPs: (d) No. II, (e) No. V and (f) No. VIII. (g) The comparison results of FEA and optical images of the MP under different deformations. The scale bar is 20 mm.

Table 1. The parameters of the elastic-plastic model of PLA-SMP.

True stress/MPa	Plastic strain/%	True stress/MPa	Plastic strain/%	True stress/MPa	Plastic strain/%	True stress/MPa	Plastic strain/%
21.21	0	38.03	0.16	46.48	0.63	46.93	0.85
23.31	0.01	39.08	0.19	46.53	0.64	46.95	0.86
24.06	0.015	40.06	0.21	46.57	0.66	46.96	0.88
25.04	0.02	41.02	0.23	46.62	0.67	46.97	0.89
26.02	0.03	41.12	0.23	46.66	0.68	46.98	0.91
27.10	0.03	42.05	0.26	46.69	0.70	46.99	0.92
28.02	0.04	43.03	0.30	46.73	0.71	47.00	0.94
29.07	0.05	44.04	0.35	46.77	0.72	47.01	0.95
30.01	0.06	45.04	0.43	46.79	0.74	47.02	0.96
31.03	0.07	46.06	0.55	46.81	0.75	47.02	0.98
32.03	0.08	46.13	0.56	46.83	0.76	47.02	0.99
33.02	0.09	46.19	0.57	46.85	0.78	47.03	1.01
34.00	0.10	46.25	0.58	46.87	0.79	47.04	1.02
35.07	0.12	46.32	0.60	46.89	0.81	47.05	1.04
36.01	0.13	46.37	0.61	46.91	0.82	/	
37.03	0.15	46.43	0.62	46.92	0.84		

Table 2. Parameter values in the Ogden model.

n	μ_1	α_1	μ_2
3	−3.21	12.41	4.27
α_2	μ_3	α_3	$D_1 = D_2 = D_3$
−2.94	6.35	−24.88	0

modules were in the second configuration, i.e. No. IV-2-3, the vibration isolation frequency range of the programmed MP was 0 Hz–13.67 Hz and 306.64 Hz–365.23 Hz, figures 3(c) and S14.

For the room-temperature programming, the developed MP in the *i*-0 state could only be transformed to the remaining stable configurations by compressive deformation, and the number of the room-temperature programming configurations was limited. Since the bistable module and the combination of the compression-torsion module and the force threshold control module had 2 independent configurations, for the MP containing α bistable modules and β combination of the compression-torsion module and the force threshold control module, it had $2^{(\alpha+\beta)}$ room temperature programming configurations. In contrast to metamaterials fabricated by conventional materials, the introduction of 4D-printed SMP allowed for thermomechanical programming of metamaterials. The 4D-printed SMP mechanical metamaterials could be programmed in any one of the configurations that were able to withstand loads independently, which further increased the design freedom and the programmable range of configuration/mechanical properties. The compression-torsion modules were fabricated by 4D printing PLA-SMP, which enabled the configurations and mechanical properties of the MP to be changed after fabrication. The specific implementation process of shape memory programming and reconfiguration of mechanical metamaterials was as follows (movie-S1). (a) Heating and loading: the compression-torsion module in the MP was heated above the glass transition temperature (T_g), and then the load was applied to deform it ($\varepsilon_{\text{stretch}}$, stretch load was applied in this work). In this deformation process, the deformation mainly occurred in the ligaments of the compression-torsion modules, so the parameters controlling the ligament configuration changed from L, R_α, ω, and ξ to L', $R_\alpha{}'$, ω', and ξ'. (b) Cooling and unloading: the applied load was held to maintain this deformation while the temperature of the MP was reduced to the room-temperature. After cooling and unloading, the MP could be fixed in this programmed configuration (i.e. $\varepsilon_{\text{target}}$). During this process, the parameters of the compression-torsion module changed from L', $R_\alpha{}'$, ω', and ξ' to L'', $R_\alpha{}''$, ω'', and ξ'' due to the partial elastic recovery after unloading. (c) Independent bear load (i.e., programmability): the MP in the programmed configuration could independently withstand external loads and exhibit different mechanical properties to the initial configuration (i.e. programmability of mechanical properties) due to the change in the geometrical parameters of the MP. (d) Heating and recovery: when the temperature of the MP was reheated above T_g, the configuration and geometrical parameters of the MP recovered to their initial state, resulting in the mechanical properties recovering to their initial state (i.e. reconfigurability).

Figures 3(e) and (f) and section-S3 exhibit the programmable performance of the displacements-force-torsion angles of the MPs. Compared with the unprogrammed MP, the programmed MP had a wider compression-torsion dominant deformation range and a lower initial effective stiffness under compression deformation, which was caused by the larger spacing between the plugs and the force threshold control module of the programmed MP. The node spacing of the programmed MP No. I and No. II increased, resulting in it exhibiting a larger torsion angle in the first compression-torsion coupling deformation domain, figures 3(e), S11(a) and (b). After the plug was contacted with the force threshold control module, the MP entered the multistable deformation domain and the torsion angle of the MP did not change with the increase of deformation. The plug was subsequently inserted into the force threshold control module and the MP's compression-torsional deformation characteristics were activated until inserted into the rotary stopping device. Figures 3(f), S11(c) and (d) exhibit the displacement-force-torsion angle behavior of the programmed MP No. VII and No. VIII (compression-torsion modules with left-handed and right-handed modes). The PMM consisting of tension-torsion coupled MPs designed in previous work exhibited low stiffness and high flexibility, which was potentially promising for application in protection devices with cushioning properties [16]. However, the PMM designed in the previous work could protect the object by cushioning and could not dissipate energy, resulting in the instantaneous release of energy after cushioning. In addition, the configuration of the flexible structure resulted in the low load carrying capacity. Although PMMs consisting of multistable MPs were capable of energy absorption through negative stiffness properties, the force–displacement curves tended to increase linearly until the $F_{\max}$ of the multistable structure was reached, which might lead to the damage of fragile objects [16, 19]. In contrast, the MP developed in this work exhibited an initial low stiffness after shape memory programming, which could provide cushioning to protect vulnerable objects from damage. In addition, the deformation of the bistable modules could store the impact energy, which effectively prevented the immediate release of energy after impact.

The PMM was obtained by tiling (m, n) the developed MP in the (x, y) directions, having $32^{(m\times n)}$ stable and reversible room temperature programmed configurations. In this work, the PMM (m, n) = (3, 3) was developed, which contained 9 multifunctional MPs and a frame (polymethyl methacrylate, PMMA), and the bottom of the MP was connected to the frame (figures 4(a) and (b)). The developed PMM had 32^9 room temperature programmed configurations. In addition, the shape memory properties further increased the design freedom of the metamaterial. Figures 4(c) and (d) exhibit PMMs composed of MP No. II and No. IV respectively, and programmed to different room temperature configurations, i.e. PMM_I–PMM_VIII, section-S4. In the unprogrammed state, the PMM exhibited a wide range of compressive deformation. The bistable modules of the developed

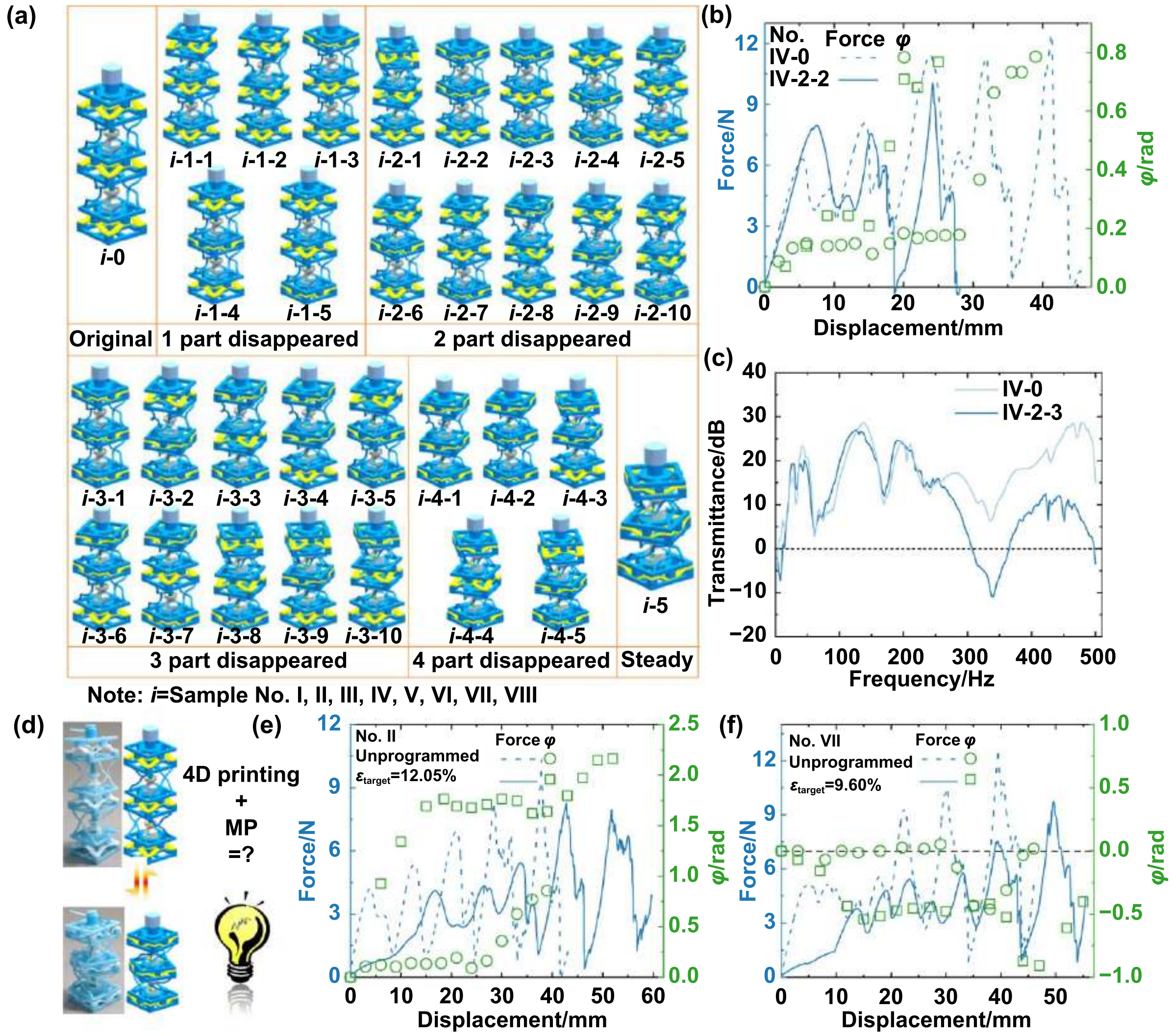

Figure 3. The programmable properties of the MP. (a) The MP had 32 independent room temperature programmable configurations. (b) Mechanical properties test of MP No. IV before and after programming (IV-0 vs. IV-2-2). (c) Transmittance of MP No. IV before and after programming (IV-0 vs. IV-2-3). (d) How the introduction of 4D printing into the manufacturing process of MP affects the properties of metamaterials. The shape memory programmable properties of mechanical properties of the MPs: (e) No. II and (f) No. VII.

PMM first deformed to these second stable configurations. Then, the plug of the MPs squeezed the force threshold control modules until they switched from ON to OFF. During compression, the PMM dissipated/stored the external compressed energy via multistable deformations and state transitions of the force threshold control modules, and thus, it exhibited energy absorption characteristics (figures 4(e)–(g)). Due to the different activation force values of the force threshold control module and the bistable module, the PMM also exhibited gradient energy absorption characteristics (i.e. first the bistable modules absorbed energy, and then the combined force threshold control modules and compression-torsion modules absorbed energy). The mechanical behavior (displacement-load curve/energy absorption characteristics) of the PMM could be adjusted by programming the MPs. For example, the energy absorption (EA) of PMM_I with the unprogrammed configuration was ~3.91 J. When all the force threshold control modules were OFF, i.e., PMM_{II}, the EA of the PMM was ~1.01 J; when all the bistable modules were in the second steady state, i.e., PMM_{III}, the EA of the PMM was ~1.91 J.

2.3. The application prospects of the MP in logic gates

The bistable modules and the combination of the compression-torsion module and the force threshold control module both exhibited two configurations, which can be encoded as two bits in binary computing. The MP with a bistable module (A) and a combination of the compression-torsion module and the force threshold control module (B) was integrated, figure 5(a). The A with the initial configuration and the B in the ON state were defined as 'close (i.e. 0)', and the A with the second stable configuration and the B in the OFF state were defined as 'open (i.e. 1)'. Therefore, the MP shown in figure 5(a) had four digital readouts, namely (A, B) = (0, 0), (1, 0), (0, 1) and (1, 1).

Mechanical logic gates can be designed through the four states of (A, B) and implement all digital logic gates and

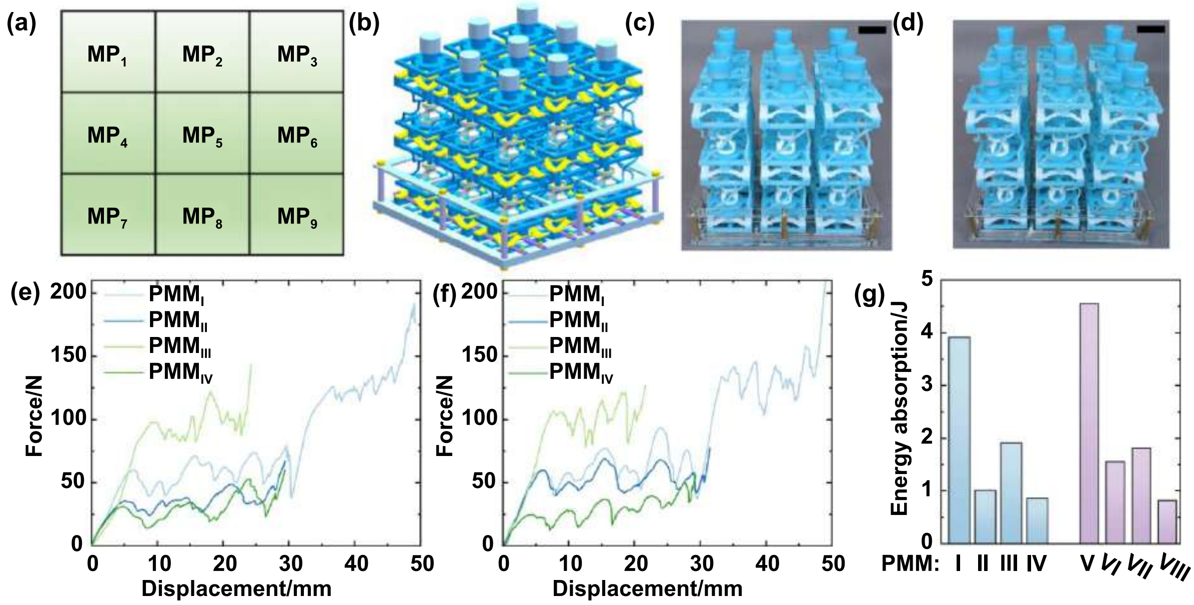

Figure 4. The programmable properties of the PMM. (a) PMM was obtained by arraying MPs along the transverse and longitudinal directions. (b) CAD model of PMM with $(m, n) = (3, 3)$. Optical images of the PMM: (c) PMM_I and (d) PMM_V. Compression performances of the PMM: (e) PMM_I–PMM_{IV} and (f) PMM_V–PMM_{VIII}. (g) Programmability of energy absorption of the developed PMM. The scale bar is 20 mm.

compute Boolean logic operations. To verify this functionality, 6 standard logic gates (i.e. AND, OR, NAND, NOR, XOR, and XNOR) were designed to utilize configuration conversion of MP and tunable circuits (figures 5(b) and S18). Ag and Cu were coated on the MP surface to enable the conduction of the circuit, figure S19. The logic gates were designed as two-layer digital units. The input A and B of the logic gate were the configuration conversion of the bistable module and the combination of the compression-torsion module in the MP, respectively, and controlled the conduction and non-conduction of the circuit. The motion changes of each layer (A and B) were either '0' or '1'. The output was the ON (1) or OFF (0) of the LED, which was powered by an external DC power (~4.5 V). By adjusting the circuit design, different mechanical inputs will produce different outputs, thus performing logical operations. Figures 5(c)–(h) and movie-S3 show the output of the 6 logic gates under different input conditions. Taking the XNOR gate as an example, when the input (A, B) = (0, 0), (1, 0), (0, 1), (1, 1), the output Q_{XNOR} was 1, 0, 0, 1, respectively. The logic gates designed in this work realized '0' or '1' input through two stable configurations of each module, which could be maintained in this input state without holding external forces. The logic gates developed in this work were more maneuverable and convenient than the logic gates that utilized constant external force to maintain the logic input state [44].

2.4. The application prospects of the PMM in energy absorbing devices

PMM demonstrated great potential for application in the field of programmable protection devices by utilizing multiple dissipation or absorption mechanisms. Truck models with different masses (1.420 kg, 5.025 kg and 7.546 kg) slid down a ~400 mm high ramp and impacted onto the PMM (PMM_V, PMM_{VI}) after sliding ~1 086 mm, to visually verify the programmable protection ability of the metamaterial, figures 6(a) and (b). In the impact process, the PMM dissipated part of the impact energy brought by the truck model via the multistability/force threshold control module, and then the truck model reversed to varying degrees under inertia, figures 6(c)–(j), section-S4 and movie-S4.

The impact load did not activate the bistable modules/force threshold control modules of the MPs after the truck model (1.420 kg) impacted the PMM_V, figures 6(c) and (g). Thus, the energy was dissipated/stored only by the friction between the plugs and the force threshold control modules/elastic deformation of the MP. As the mass of the truck model increased ~253.87% and 431.41% to 5.025 kg and 7.546 kg, respectively, part of the bistable module/force threshold control module of the MP was activated, figures 6(d)–(i). Multiple energy dissipation mechanisms of the PMM were also activated, and as a result, the backset of the truck model was similar to that before the addition of mass. When all the force threshold switching modules in the PMM were OFF, the PMM dissipated energy only by multistable deformation. Therefore, when the truck model (5.025 kg) impacted PMM_{VI}, the truck produced a large backward movement, figures 6(f) and (j). Compared with our previous work [16], the maximum weight of the impact object tested in this work was 7.546 kg, which is 109.61 times higher. Compared to our previously designed PMM consisting of tension-torsional coupled MP [16], the metamaterials developed in this work were capable of storing the impact energy through bistable modules, which improved the impact resistance of the metamaterials. In addition, the shape memory programmed MP exhibited a lower initial effective stiffness (figures 3(e) and (f)), which was

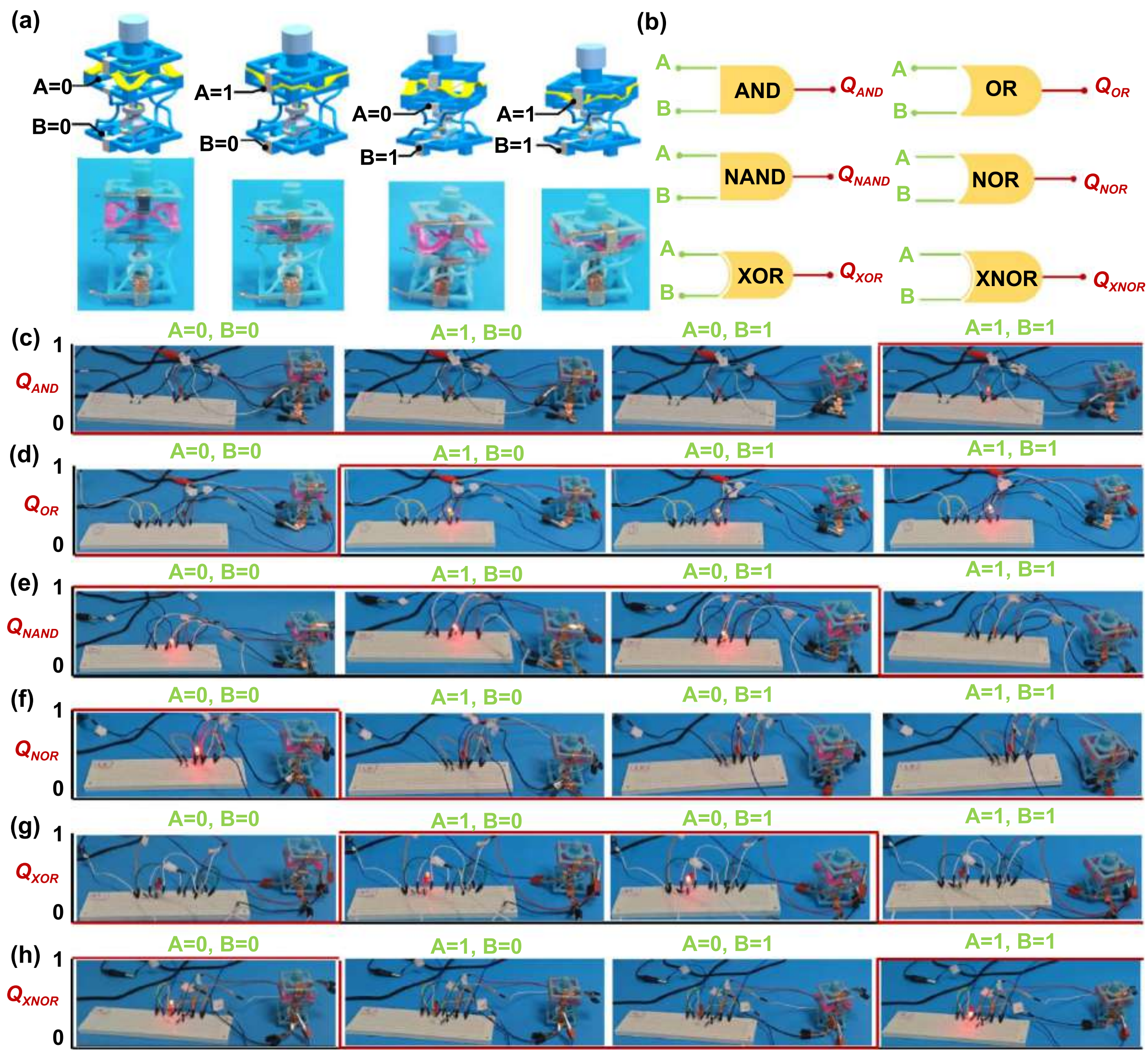

Figure 5. The design of MP-based logic gates. (a) The bistable module (A) and the combination of the compression-torsion module and the force threshold control module (B) exhibit 4 states, i.e. (A, B) = (0, 0), (1, 0), (0, 1) and (1, 1). (b) Six logic gates: AND, OR, NAND, NOR, XOR, and XNOR. The output of the 6 logic gates under different input conditions: (c) AND, (d) OR, (e) NAND, (f) NOR, (g) XOR, and (h) XNOR.

able to provide cushioning for fragile objects to prevent damage. Importantly, the developed PMM could be reused after impact, and even if some MPs were damaged, the modular design concept enabled rapid reconstruction and repair of the metamaterial. The PMM offered a new concept for designing re-usable energy absorbing materials in the fields of personnel protection, collision mitigation of automobiles and aircraft, and protective packaging of precision components.

3. Conclusion

In summary, we demonstrated the performance of the multifunctional PMM with reprogrammable properties. By controlling the force threshold, the developed metamaterial enabled a controlled transition between multistable deformation and compression-torsion coupled deformation. The MP exhibited 32 stable and reversible programmable configurations, and the PMM integrated by the MP had $32^{(m \times n)}$ programmed configurations. 4D printing further increased the programmability and design freedom of the metamaterials. Due to the modularity, the mortise and tenon joints, we believe that the developed metamaterial can be constructed on a large scale. In addition, this multifunctional design strategy, which allowed for controllable transformation between multiple extraordinary mechanical properties, can be extended to other mechanical metamaterials to promote a new generation of metamaterials with multifunctionality and personalization.

4. Experimental section

(1) **The fabrication method of the compression-torsion module:** the CAD models of the compression-torsion module were built by Siemens PLM Software UG NX10.0,

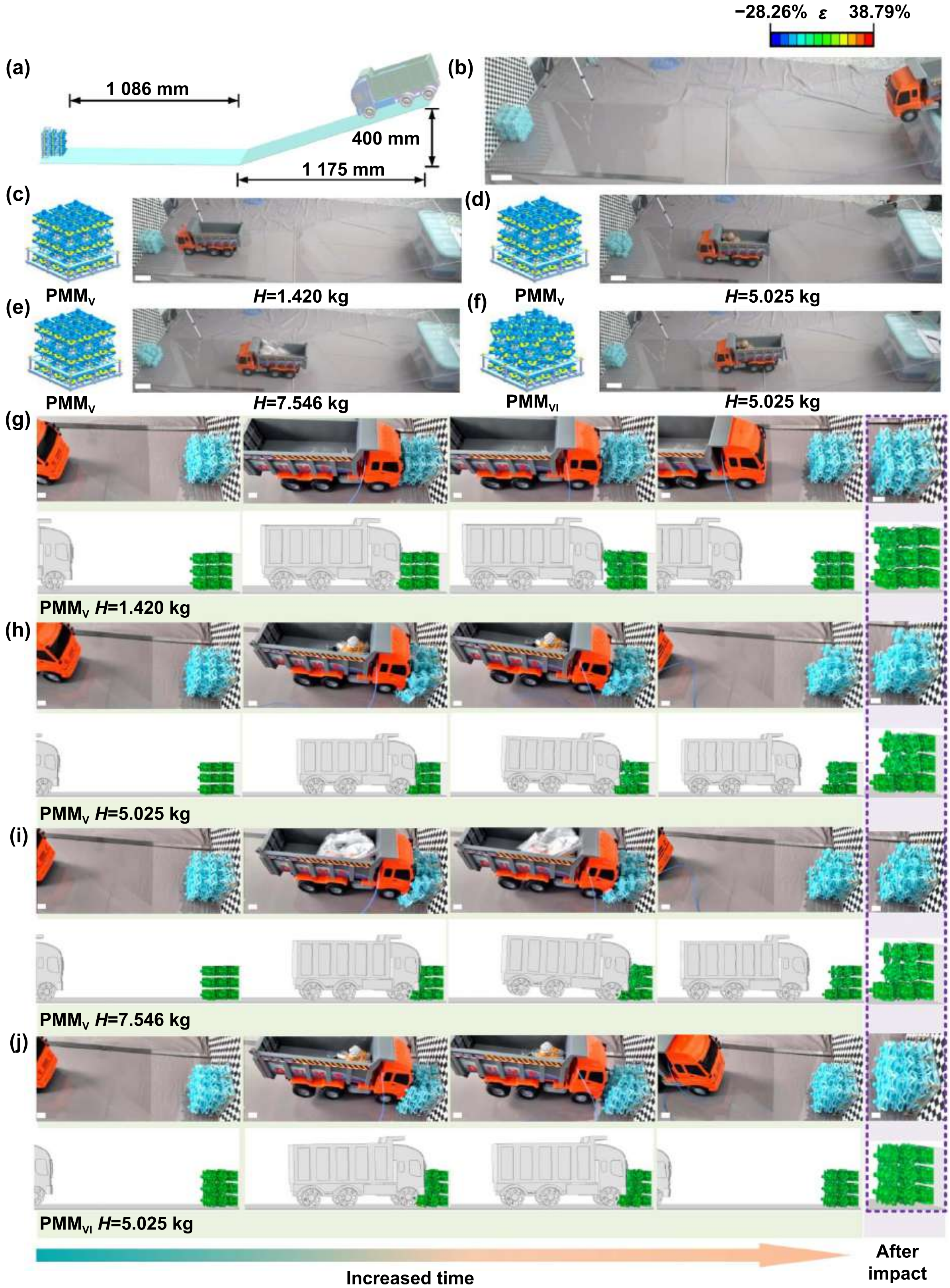

Figure 6. Truck model impact test. (a) Schematic diagram. (b) Optical images. The stopping positions of truck models with different masses colliding with PMM_V: (c) 1.420 kg, (d) 5.025 kg, and (e) 7.546 kg. (f) The stopping positions of a truck (5.025 kg) after colliding with PMM_{VI}. The process of truck models with different masses colliding with PMM_V: (g) 1.420 kg, (h) 5.025 kg, and (i) 7.546 kg. (j) The process of truck (5.025 kg) colliding with PMM_{VI}. The scale bars in (b)-(f) are 140 mm. The scale bars in (g)–(j) are 30 mm.

and the file was exported in '.stl' format. Then, this file was extracted in Anycubic Photon Workshop 64 to obtain the cross-section images of the print model. The compression-torsion modules were fabricated utilizing the Anycubic Photon M3 Plus 3D printer. The 3D printer utilized an LCD panel to tune the UV light, which selectively transmitted UV light generated from light-emitting diodes (LEDs) with 405 nm wavelength, and then focused on the surface of the shape memory polylactic acid (PLA-SMP) photosensitive resin in the bath. After one layer was photopolymerized, the platform moved the printed sample upward and the next layer was photopolymerized on the top of the previous layer. Repeat this process to build the compression-torsion module layer by layer until all layers were printed. The exposure time and photopolymerized thickness of each layer were 2.5 s and 0.05 mm, respectively.

(2) **The fabrication method of the bistable module and the force threshold control module:** the CAD models of the bistable module and the force threshold control module were built by Siemens PLM Software UG NX10.0, and the file was exported in '.stl' format. These two modules were fabricated by the Anycubic Mega-x fused deposition modeling (FDM) 3D printer, utilizing TPU as the printing filament. The temperature of the build platform and extrusion nozzle was set to 40 °C and 220 °C respectively, and the print filament was deposited on the platform at the rate of 5 mm $\min^{-1}$. The printer first heated the print platform and the extrusion nozzle to the predefined temperature before printing. The stepper motor extruded the print filament (diameter ~1.75 mm) from the circular nozzle (diameter ~0.4 mm) at the set print speed and deposited it on the print platform. While extruding the printed filament, the stepper motor on the cross beam drove the extrusion nozzle movement to print the design module.

(3) **The fabrication of the MP and PMM:** the MP was assembled gradually by inserting the tenons of each module into the mortises as shown in the schematic diagram of figure 1(d). After assembling, the MP's modules were connected firmly by applying glue to the joints. The MPs were placed into the PMMA frame and assembled into the PMM.

(4) **Mechanical properties of the PLA-SMP:** the thermomechanical properties of the PLA-SMP have been described in detail in our previous work [16, 26]. The glass transition temperature (T_g), Young's modulus, and elongation of the PLA-SMP were ~70.60 °C, ~1.4 GPa, and ~9% (25 °C), respectively. In the FEA, the elastic-plastic model was employed to simulate the deformation behavior of PLA-SMP at room temperature.

(5) **Mechanical properties of the TPU:** the room temperature uniaxial tensile properties of TPU dumbbell-shaped specimens (115 mm × 6 mm × 2 mm) fabricated by FDM were characterized on the Zwick-010 tensile machine, the deformation rate and maximum strain was 5 mm $\min^{-1}$ and 60%, respectively. The Ogden model can accurately describe the hyperelastic deformation behavior of TPU at room temperature (supporting information, figure S4). The form of the Ogden strain energy potential was:

$$U = \sum_{i=1}^{n} \frac{2\mu_i}{\alpha_i^2}\left(\bar{\lambda}_1^{\alpha_i} + \bar{\lambda}_2^{\alpha_i} + \bar{\lambda}_3^{\alpha_i} - 3\right) + \sum_{i=1}^{n} \frac{1}{D_i}\left(J^{e\ell} - 1\right)^{2i} \ldots (n = 3 \text{ in this work}) \quad (1)$$

where $\bar{\lambda}_i$ were the deviatoric principal stretches, $\bar{\lambda}_i = J^{-\frac{1}{3}}\lambda_i$; λ_i was the principal stretches; n, μ_i, α_i, and D_i were material parameters. The initial shear modulus and bulk modulus for the Ogden form were:

$$\mu_0 = \sum_{i=1}^{N} \mu_i, K_0 = \frac{2}{D_1}. \quad (2)$$

In this work, Ogden strain energy potential was $n = 3$, where the values of μ_i, α_i, and D_i are shown in table 2.

(6) **Compression mechanical properties characterization method:** the nonlinear mechanical behaviors of each module and metamaterial were investigated at 5 mm $\min^{-1}$ in the Zwick-010 tensile machine. During the test, the deformation process was recorded by the camera (Canon ds126571). The normal mode (1 080 p and 30 fps) and slow motion mode (720 p and 240 fps) of the camera were employed to record the collision process of the truck model.

(7) **FEA:** ABAQUS (SIMULIA)/Explicit was employed to perform simulation analysis of compression-torsion modules, the MPs, and impact tests.

(8) **Vibration Testing:** during dynamic testing, the MP No. II and IV with programmed and unprogrammed configurations were assembled onto an electromechanical shaker, figure S14(a). The shaker provided a white noise input signal over the broadband frequency range. Two accelerometers were connected to the two ends of the sample (bottom and top of the MP) for receiving the input and output signals to measure the transmittance of the sample versus the frequency of the incident wave. The white noise signal was generated by the signal generation module included in the dynamic signal collection system, and then amplified by the power amplifier. The acceleration signals were measured by the dynamic signal collection system.

Acknowledgments

The authors gratefully acknowledge the financial support provided by the National Key R&D Program of China (2022YFB3805700), the National Natural Science Foundation of China (Grant Nos. 12072094 and 12172106), the China Postdoctoral Science Foundation (Grant No. 2023M730869), the Heilongjiang Natural Science Foundation Joint Guidance Project (Grant No. LH2023A004), the Postdoctoral Fellowship Program of CPSF (Grant No. GZB20230959).

ORCID iD

Yanju Liu https://orcid.org/0000-0001-8269-1594

References

[1] Shelby R A, Smith D R and Schultz S 2001 Experimental verification of a negative index of refraction *Science* **292** 77–79
[2] Clausen A, Wang F W, Jensen J S, Sigmund O and Lewis J A 2015 Topology optimized architectures with programmable Poisson's ratio over large deformations *Adv. Mater.* **27** 5523–7
[3] Liu J X, Yan D J and Zhang Y H 2021 Mechanics of unusual soft network materials with rotatable structural nodes *J. Mech. Phys. Solids* **146** 104210
[4] Mei T, Meng Z Q, Zhao K J and Chen C Q 2021 A mechanical metamaterial with reprogrammable logical functions *Nat. Commun.* **12** 7234
[5] Meza L R, Zelhofer A J, Clarke N, Mateos A J, Kochmann D M and Greer J R 2015 Resilient 3D hierarchical architected metamaterials *Proc. Natl Acad. Sci. USA* **112** 11502–7
[6] Berger J B, Wadley H N G and McMeeking R M 2017 Mechanical metamaterials at the theoretical limit of isotropic elastic stiffness *Nature* **543** 533–7
[7] Coulais C, Sounas D and Alù A 2017 Static non-reciprocity in mechanical metamaterials *Nature* **542** 461–4
[8] Zheng X Y *et al* 2014 Ultralight, ultrastiff mechanical metamaterials *Science* **344** 1373–7
[9] Tan C L, Deng C, Li S, Abena A, Jamshidi P, Essa K, Wu L K, Xu G H, Attallah M M and Liu J 2022 Mechanical property and biological behaviour of additive manufactured TiNi functionally graded lattice structure *Int. J. Extrem. Manuf.* **4** 045003
[10] Zhang W Q, Ye H T, Feng X B, Zhou W Z, Cao K, Li M Y, Fan S F and Lu Y 2022 Tailoring mechanical properties of PμSL 3D-printed structures via size effect *Int. J. Extrem. Manuf.* **4** 045201
[11] Huang Y H *et al* 2023 A direct laser-synthesized magnetic metamaterial for low-frequency wideband passive microwave absorption *Int. J. Extrem. Manuf.* **5** 035503
[12] Li X, Peng W T, Wu W W, Xiong J and Lu Y 2023 Auxetic mechanical metamaterials: from soft to stiff *Int. J. Extrem. Manuf.* **5** 042003
[13] Xu R, Chen C Q, Sun J P, He Y L, Li X, Lu M H and Chen Y F 2023 The design, manufacture and application of multistable mechanical metamaterials-a state-of-the-art review *Int. J. Extrem. Manuf.* **5** 042013
[14] Frenzel T, Kadic M and Wegener M 2017 Three-dimensional mechanical metamaterials with a twist *Science* **358** 1072–4
[15] Tao R, Ji L T, Li Y, Wan Z S, Hu W X, Wu W W, Liao B B, Ma L H and Fang D N 2020 4D printed origami metamaterials with tunable compression twist behavior and stress-strain curves *Composites* B **201** 108344
[16] Xin X Z, Liu L W, Liu Y J and Leng J S 2022 4D pixel mechanical metamaterials with programmable and reconfigurable properties *Adv. Funct. Mater.* **32** 2107795
[17] Librandi G, Tubaldi E and Bertoldi K 2021 Programming nonreciprocity and reversibility in multistable mechanical metamaterials *Nat. Commun.* **12** 3454
[18] Melancon D, Gorissen B, García-Mora C J, Hoberman C and Bertoldi K 2021 Multistable inflatable origami structures at the metre scale *Nature* **592** 545–50
[19] Pan F, Li Y L, Li Z Y, Yang J L, Liu B and Chen Y L 2019 3D pixel mechanical metamaterials *Adv. Mater.* **31** 1900548
[20] Chen T, Pauly M and Reis P M 2021 A reprogrammable mechanical metamaterial with stable memory *Nature* **589** 386–90
[21] Coulais C, Teomy E, de Reus K, Shokef Y and van Hecke M 2016 Combinatorial design of textured mechanical metamaterials *Nature* **535** 529–32
[22] Silverberg J L, Evans A A, McLeod L, Hayward R C, Hull T, Santangelo C D and Cohen I 2014 Using origami design principles to fold reprogrammable mechanical metamaterials *Science* **345** 647–50
[23] Zhang H, Wu J, Fang D N and Zhang Y H 2021 Hierarchical mechanical metamaterials built with scalable tristable elements for ternary logic operation and amplitude modulation *Sci. Adv.* **7** eabf1966
[24] Yan D J, Chang J H, Zhang H, Liu J X, Song H L, Xue Z G, Zhang F and Zhang Y H 2020 Soft three-dimensional network materials with rational bio-mimetic designs *Nat. Commun.* **11** 1180
[25] Yang C, Boorugu M, Dopp A, Ren J, Martin R, Han D, Choi W and Lee H 2019 4D printing reconfigurable, deployable and mechanically tunable metamaterials *Mater. Horiz.* **6** 1244–50
[26] Xin X Z, Liu L W, Liu Y J and Leng J S 2020 4D printing auxetic metamaterials with tunable, programmable, and reconfigurable mechanical properties *Adv. Funct. Mater.* **30** 2004226
[27] Hamzehei R, Serjouei A, Wu N, Zolfagharian A and Bodaghi M 2022 4D metamaterials with zero Poisson's ratio, shape recovery, and energy absorption features *Adv. Eng. Mater.* **24** 2200656
[28] Wu J, Yao S L, Zhang H, Man W T, Bai Z L, Zhang F, Wang X M, Fang D N and Zhang Y H 2021 Liquid crystal elastomer metamaterials with giant biaxial thermal shrinkage for enhancing skin regeneration *Adv. Mater.* **33** 2106175
[29] Lendlein A and Gould O E C 2019 Reprogrammable recovery and actuation behaviour of shape-memory polymers *Nat. Rev. Mater.* **4** 116–33
[30] van Manen T, Janbaz S, Jansen K M B and Zadpoor A A 2021 4D printing of reconfigurable metamaterials and devices *Commun. Mater.* **2** 56
[31] Zhang B *et al* 2021 Mechanically robust and UV-curable shape-memory polymers for digital light processing based 4D printing *Adv. Mater.* **33** 2101298
[32] Xia Y L, He Y, Zhang F H, Liu Y J and Leng J S 2021 A review of shape memory polymers and composites: mechanisms, materials, and applications *Adv. Mater.* **33** 2000713
[33] Zhao Q, Qi H J and Xie T 2015 Recent progress in shape memory polymer: new behavior, enabling materials, and mechanistic understanding *Prog. Polym. Sci.* **49–50** 79–120
[34] Gu J P, Zhang X P, Duan H, Wan M Q and Sun H Y 2021 A hygro-thermo-mechanical constitutive model for shape memory polymers filled with nano-carbon powder *Int. J. Smart Nano Mater.* **12** 286–306
[35] Zhang W *et al* 2021 Structural multi-colour invisible inks with submicron 4D printing of shape memory polymers *Nat. Commun.* **12** 112
[36] Lin C, Lv J X, Li Y S, Zhang F H, Li J R, Liu Y J, Liu L W and Leng J S 2019 4D-printed biodegradable and remotely controllable shape memory occlusion devices *Adv. Funct. Mater.* **29** 1906569
[37] Lee S, Bang D, Park J O and Choi E 2022 Programmed shape-morphing material using single-layer 4D printing system *Micromachines* **13** 243
[38] Kuang X, Roach D J, Wu J T, Hamel C M, Ding Z, Wang T J, Dunn M L and Qi H J 2019 Advances in 4D printing: materials and applications *Adv. Funct. Mater.* **29** 1805290

[39] Fu P *et al* 2022 4D printing of polymers: techniques, materials, and prospects *Prog. Polym. Sci.* **126** 101506
[40] Lee A Y, An J and Chua C K 2017 Two-way 4D printing: a review on the reversibility of 3D-printed shape memory materials *Engineering* **3** 663–74
[41] Rafiee M, Farahani R D and Therriault D 2020 Multi-material 3D and 4D printing: a survey *Adv. Sci.* **7** 1902307
[42] Zhou X L, Ren L Q, Song Z Y, Li G W, Zhang J F, Li B Q, Wu Q, Li W X, Ren L and Liu Q P 2023 Advances in 3D/4D printing of mechanical metamaterials: from manufacturing to applications *Composites* B **254** 110585
[43] Xu P L, Lan X, Zeng C J, Zhang X D, Zhao H X, Leng J S and Liu Y J 2024 Compression behavior of 4D printed metamaterials with various Poisson's ratios *Int. J. Mech. Sci.* **264** 108819
[44] El Helou C, Buskohl P R, Tabor C E and Harne R L 2021 Digital logic gates in soft, conductive mechanical metamaterials *Nat. Commun.* **12** 1633